Hydrodynamic and rheological characteristics of a pseudoplastic fluid through a rotating cylinder

Mohamed Abdi, Meryem Ould-Rouiss, Abdelkader Noureddine

▶ **To cite this version:**

Mohamed Abdi, Meryem Ould-Rouiss, Abdelkader Noureddine. Hydrodynamic and rheological characteristics of a pseudoplastic fluid through a rotating cylinder. Numerical Heat Transfer, Part A Applications, 2023, pp.1-20. 10.1080/10407782.2023.2181894 . hal-04075347

HAL Id: hal-04075347
https://hal.science/hal-04075347

Submitted on 7 Jun 2023

HAL is a multi-disciplinary open access archive for the deposit and dissemination of scientific research documents, whether they are published or not. The documents may come from teaching and research institutions in France or abroad, or from public or private research centers.

L'archive ouverte pluridisciplinaire **HAL**, est destinée au dépôt et à la diffusion de documents scientifiques de niveau recherche, publiés ou non, émanant des établissements d'enseignement et de recherche français ou étrangers, des laboratoires publics ou privés.

Hydrodynamic and Rheological Characteristics of a Pseudoplastic Fluid Through a Rotating Cylinder

Mohamed Abdi [a], Meryem Ould-Rouiss [b] and Abdelkader Noureddine [c]

[a] Laboratoire de génie électrique et des plasmas (LGEP) University of Tiaret, Algeria
[b] Laboratoire de Modélisation et Simulation Multi Echelle, MSME, Université Gustave Eiffel, UMR 8208 CNRS, 5 bd Descartes, 77454 Marne-la-Vallée, Paris, France
[c] Laboratoire de Mécanique Appliquée, Université USTO Mohamed Boudiaf, BP 1505 Oran EL M'Naouar, Oran, Algeria

Address correspondence to Mohamed Abdi
E-mail: abdi.mohamed1@live.fr

Abstract

The fully developed turbulent flow of pseudoplastic ($n = 0.75$) and Newtonian fluids in an isothermal axially rotating cylinder has been carried out using a large eddy simulation (LES) with an extended Smagorinsky model. The simulation Reynolds number of the present predictions has been assumed to be $\mathrm{Re}_s = 4000$ at various rotation rates $(0 \le N \le 3)$. This investigation seeks to assess the influence of the centrifugal force induced by the swirl on the mean flow quantities, turbulent statistics, and instantaneous turbulence structure to describe the rheological behavior and the turbulence features. The predicted results indicate that with increasing rotation rate, the pseudoplastic fluid tends to behave like a liquid when approaching the pipe center due to the lower apparent fluid viscosity in the logarithmic region as the pipe wall rotates. Moreover, the reduction in the pseudoplastic apparent viscosity in the core region induces a pronounced increase in the axial velocity profile further away from the pipe wall toward the core region. It is interesting to note that the growth of the centrifugal force induced by the swirl driven by the rotating pipe wall results in an apparent attenuation in turbulence intensities of the axial velocity fluctuation and, consequently, in the kinetic energy of turbulent fluctuations and the turbulent Reynolds shear stress of the axial-radial velocity fluctuations, as the pipe wall rotates. Moreover, the increased rotation rate leads also to a noticeable increase in the Root mean square (RMS) of the radial and tangential fluctuations. It can be said that the transport mechanism of turbulence intensities from the axial components to the other ones exhibits a marked increase with increasing pipe wall rotation.

Keywords: LES; Non-Newtonian; Pseudoplastic fluid; Turbulent flow; Rotating cylinder

1. Introduction:

Flow in swirling systems is not only of great importance to practical applications in mechanical and engineering fields (heat exchangers, combustion chambers, nuclear reactors, and turbomachines) but also of considerable fundamental interest. To better understand the laminarization phenomena and analyze the influence of the rotation pipe wall on the mean properties and turbulence statistics, many authors performed experimental [1], [2], [3], [4], and [5], theoretical and numerical [6], [7], [8], [9] and [10] studies. But most of them are based on the turbulent flow of Newtonian fluids. They found that the rotating pipe wall significantly influences the turbulence due to the centrifugal force, which has a stabilizing effect: the increased rotation velocity of the cylinder wall results in a pronounced increase in the mean axial velocity profile along the radial coordinate, where this profile progressively approaches to a laminar one; this is called the laminarization phenomena.

However, relatively few works focused on non-Newtonian fluids, whose viscosity depends on the shear rate. Some authors conducted theoretical and experimental investigations devoted to the turbulent flow of non-Newtonian fluids flow through a straight axial pipe [11], [12], [13], and [14]. To provide detailed information on the turbulence statistics and flow characteristics, numerical investigations were performed [15], [16], [17], [18], [19], [20], [21], and [22]. In their paper, Dodge and Metzner [13] developed for the first time a theoretical study for the Non-Newtonian fluids in turbulent flow through straight cylinders; they derived a semi-theoretical expression for the pressure loss and mean flow rate and predicted the non-Newtonian turbulent velocity profiles, as well as a correlation for friction factor. In 1990, Pinho and Whitelaw [14] measured the streamwise velocity and the three normal stresses for the Non-Newtonian fluids in a fully developed flow for a Reynolds number ranging from 240 to 111000. Malin [15] investigated numerically the fully developed laminar and turbulent flows of shear-thinning, Newtonian, and shear-thickening fluids in a straight cylinder, at various values of Reynolds numbers, using a modified version of the Lam-Bremhorst $K-\varepsilon$ Model for the turbulent flow.

Rudman et al. [16] reported one of the first numerical attempts to provide some important insights into the turbulence features and flow behavior of the shear-thinning and Herschel-Bulkley fluids through an isothermal axially pipe at different generalized Reynolds numbers. Their emerged predicted results suggest that the decreased flow behavior index results in a pronounced increase in the axial velocity profile further away from the pipe wall, and a reduction in the friction factor, due to the higher apparent viscosity of the shear-thinning fluid in the flow core region. Gnambode et al.[17] implemented a LES technique with an extended Smagorinsky model to perform numerically the turbulent flow of pseudoplastic and dilatant fluids with flow behavior index ranging from 0.5 to 1.4 at different Reynolds numbers (4000, 8000, and 12000). The findings suggest that the increased Reynolds number increases the velocity profiles along the pipe radius, especially in the logarithmic

flow region. The friction factor decreases noticeably as the flow behavior index is decreased, while this friction also decreases with increasing Reynolds number for both shear-thinning and shear-thickening fluids. Moreover, a clear trend of decrease in the apparent fluid viscosity when approaching the core region when the flow behavior index is increased. Gavrilova and Rudyak [18], [19] provided an extensive investigation of DNS of fully developed turbulent pipe flows of shear-thinning ($0.4 \leq n \leq 1$) fluids at two generalized Reynolds numbers 10000 and 20000. To critically assess the effects of the flow behavior index and the Reynolds number on the main turbulence features and the rheological behavior. The relevant predicted results are in accord with Rudman et al. [16] study, indicating that the decreased flow behaviour index results in a pronounced increase of the apparent fluid viscosity further away from the pipe wall towards the pipe core region, where the shear-thinning tends to behave like a solid when approaching to the pipe centre. Which leads to increase the axial velocity in the core region, and attenuate significantly the friction factor [18]. It is observed that with decreasing flow behavior index, the fluctuations of the radial and tangential velocity components exhibit marked attenuation. This deviation leads to an increase of the axial fluctuations, consequently integral fluctuations and kinetic energy of turbulent fluctuations. Singh et al. (2017) [20] reported a DNS investigation of turbulent power-law fluids across the axially stationary pipe at a friction Reynolds number of 323 over a flow behavior index range of ($0.4 \leq n \leq 1.2$). It is found that the decreased flow behavior index leads to a marked reduction in the Reynolds shear stress where the turbulence structures become finer with decreasing flow index. Moreover, the apparent fluid viscosity of the shear-thickening fluid is lower than those of the shear-thinning fluids out of the viscous sublayer. More recently, to ensure the accuracy and efficiency of the OpenFOAM library, Zheng et al. (2019) [22] have performed numerical DNS of the fully developed turbulent flow of shear-thinning fluids through a pipe. The results show that the predicted velocity and viscosity profiles are well resolved, while the turbulence statistics have marked a noticeable difference compared with those obtained from the spectral element-Fourier DNS code. Interestingly, the turbulent intensities and Reynolds stresses profiles differ with a maximum of 16% and 10% at Reynolds numbers 5000 and 7500, respectively.

A literature survey reveals that very few studies deal with the turbulent swirling flow of non-Newtonian fluids. In contrast, the relevant numerical research aforementioned has been devoted to the turbulent flow of the non-Newtonian fluids inside a stationary pipe. Therefore, a noticeable paucity of studies describing the impact of the centrifugal force induced by the swirl driven by a rotating pipe wall on the rheological and turbulence behavior. It should be noted that the fully developed turbulent flow of the non-Newtonian fluid through the axially rotating pipe was treated theoretically by Vidyanidhi and Sithapathi [23] and theoretically and experimentally by

Gunn et al. [24]. Gunn et al. (1974) [24] provide theoretically and experimentally an extensive analysis of laminar and turbulent Newtonian and non-Newtonian fluids through an axially rotating pipe to examine the effects of the rotation rate on the flow patterns. The experiment results indicate that in the laminar flow, the flow rate of the Newtonian fluid decreases significantly when the pipe is rotating, this trend is more pronounced as the Reynolds number is increased, and the flow rate becomes nearly independent of the rotation rate at the high Reynolds number in the laminar regime. In contrast, the flow rate of the non-Newtonian exhibits a marked increase when the pipe rotates, where the rotation rate induces a gradually increase in the flow rate in the laminar regime. In the turbulent flow, the rotation rate results a slightly increase in the pressure gradient of Newtonian fluid, while that this increase is more pronounced in the non-Newtonian fluid, it is interesting to note that this enhancement is more important as the flow rate increases.

More recently, Abdi et al. [25] have performed for the first time a fully developed turbulent forced convection of thermally independent pseudoplastic fluid with a flow behavior index of 0.75 through an axially heated rotating pipe by mean of LES with an extended Smagorinsky model. With a rotation rate ranging from 0 to 3, the simulation Reynolds and Prandtl numbers of the working fluid were assumed to be 4000 and 1, respectively. It is observed that the increased rotation rate induces a marked attenuation in the temperature along the pipe radius. The centrifugal force induced by the rotating pipe wall leads to a noticeable increase in the mean axial velocity profile as the pipe wall rotates due to the reduction in the apparent fluid viscosity in the core region. It is also demonstrated that the turbulence intensities of temperature fluctuations and the axial turbulent heat flux exhibit an apparent attenuation when the pipe rotates. When the rotation rate increases, there is a clear reduction trend in the transfer mechanism of the temperature fluctuations between the conductive layer and the flow core region. Their findings indicate that the Nusselt number reduces when the rotation rate is less than 0.5, while it increases with an increasing rotation rate for N greater than 1. As for the higher-order statistics, it is demonstrated that the influence of the rotation rate on the skewness and flatness coefficients is mainly restricted in the near-wall region; these profiles seem nearly independent of the centrifugal force induced by the rotating pipe wall further away from the pipe wall.

It is clear that a comprehensive study on the turbulent pipe flow with a swirl of non-Newtonian fluids through an axially rotating pipe is still lacking for hydrodynamic and rheological investigations. To this end, under the same investigation hypothesis as that of Abdi et al. [25], the present study deals numerically with the fully developed turbulent flow through an isothermal axially rotating pipe of a pseudoplastic (n=0.75) and Newtonian fluids by mean of LES with extended Smagorinsky model. The current study set out to reveal the effects

of the centrifugal force induced by the rotating pipe wall on the hydrodynamic and rheological behavior as well as the turbulent statistics and instantaneous turbulence structure of the shear-thinning fluids, via analyzing and discussing critically the mean flow and rheological properties as well as the main turbulence characteristics.

The fluid modeled in this study is power-law (pseudoplastic) fluid, the shear stress is related to the shear rate by: $\tau = K\left(\dot{\gamma}\right)^n$, where $\dot{\gamma}$ is the shear rate K is the consistency index and n is the flow behavior index. The apparent viscosity η is not constant for the power-law fluid; a function of the magnitude of the shear rate is written in the form: $\eta = K\dot{\gamma}^{n-1}$. For $n<1$, the apparent viscosity decreases with increasing shear rate, and fluid is called shear-thinning (pseudoplastic). $n>1$, the apparent viscosity increases with the increased shear rate, and fluid is termed shear-thickening (dilatant), which the Newtonian flow behavior is expected for $n=1$. Metzner and Reed (1955) [11] were the first to propose a definition of the generalized Reynolds number of the power-law fluids based on the effective viscosity $\eta_{eff} = K\left(3n+1/4n\right)^n\left(8U/D\right)^{n-1}$; thus, the Metzner and Reed Reynolds number is defined as $\mathrm{Re}_{MR} = \rho U^{2-n}D^n \big/ 8^{n-1}K\left(3n+1/4n\right)^n$. Another commonly used generalized Reynolds number Re_g based on the apparent viscosity of the fluid at the wall $\eta_w = K\left(\dot{\gamma}_w\right)^{n-1}$, where this Reynolds number reflects the flow behavior in the vicinity of the wall. Moreover, the friction Reynolds is based on the wall friction velocity and the mean viscosity on the wall $\mathrm{Re}_\tau = \rho u_\tau D/\eta_w$. Whereas the distance from the wall in wall units Y^+ is also based on the viscosity of the fluid at the wall, it thus follows that $Y^+ = \rho y u_\tau/\eta_w$.

The present paper is organized as follows; the governing equations and numerical procedure are described in section 2. the effect of rotating pipe wall on the mean quantities and turbulent flow statistics (axial and tangential velocities, Root mean square of the fluctuating velocity, turbulent Reynolds stress and instantaneous turbulence structure), are presented in section 3. Section 4 summarizes the main findings of this study and concludes.

2. Governing equations and computational method:

2.1. Governing equations:

A large eddy simulation approach with an extended Smagorinsky model has been applied to study the turbulent flow of the pseudoplastic (n<1) fluid through a straight axially rotating cylinder of $20R$ as a length in the axial direction (see Fig.1). The flow behavior index (n) was chosen to be 0.75 at the simulation Reynolds number of 4000, and the rotation rate in this paper set out to be (N=0, 0.5, 1, 2, and 3).

The filtered equations are written as:

$$\frac{\partial \bar{u}_i}{\partial x_i} = 0 \tag{1}$$

$$\frac{\partial \bar{u}_j}{\partial t} + \frac{\partial \bar{u}_i \bar{u}_j}{\partial x_i} + \varepsilon_{ijk} N_k \bar{u}_l = -\frac{\partial \bar{p}}{\partial x_i} + \frac{1}{\mathrm{Re}_s} \frac{\partial}{\partial x_i} \left[\overline{\dot{\gamma}^{n-1}} \left(\frac{\partial \bar{u}_i}{\partial x_j} + \frac{\partial \bar{u}_j}{\partial x_i} \right) \right] - \frac{\partial \bar{\sigma}_{ij}}{\partial x_i} + \frac{\partial \bar{T}_{ij}}{\partial x_i} \tag{2}$$

Where $N_k = 2\Omega_k R / U_{CL}$ is defined as the rotation rate and Ω_k the rotational pipe wall velocity. Re_s is the Reynolds number of the simulations and is defined as $\mathrm{Re}_s = \rho U_{CL}^{2-n} R^n / K$.

2.2. Computational method:

Filtering the Navier-Stokes equations eliminates scales smaller than the filter Δ. These eliminated scales, called subgrid-scale (SGS) motions (small eddies), are unresolved small-scale fluid motions in the filtered equations that govern the resolved large-scale scales. The SGS motions' effects on the resolved scales are modeled using an eddy-viscosity closure and the strain rate tensor. According to Ohta and Miyashita, the currently filtered equations were closed by an extended Smagorinsky model, where the additional terms were ignored [26].

The present LES investigations were performed with a laboratory code; for more details on the computational procedure, see the investigation of Gnambode et al. [17]. The grid resolution 65^3 grid points in *r, z,* and θ directions, respectively, with a domain length of 20*R* in the streamwise direction, was chosen for all simulations presented in this work (this choice is based on the mesh independence study performed by Gnambode et al. [17] for *n*=0.75). We applied a non-uniform distribution grid defined by a hyperbolic tangent function in the radial direction, in addition to periodic boundary conditions and an equally spaced computational grid in the axial and the azimuthal directions.

It is worth noting that Montreuil [27] pointed out that the LES with high resolution can be carried out with Δz^+ equal to 35 wall units and $\left(r\Delta\theta\right)^+$ less than 10 wall unites, while Zang [28] reported that the adequate LES could be carried out using Δz^+ and $\left(r\Delta\theta\right)^+$ less than 80 and 40 wall units, respectively. It can be seen from the data in Tab.1 that the first grid points away from the wall in the current work are placed at $Y^+ < 1$, where the first mesh point is located at 0.0239 and 0.0241 wall units for the lowest (*N*=0) and the highest (*N*=3) rotation rate, respectively. In addition, 24 grid points at least are located within the viscous sublayer $Y^+ < 5$ for all simulations. One can also see from Tab.1 the maximum and the minimum values Δz^+ are 66.01 and 70.55 wall units, respectively, while that $r\Delta\theta^+$ ranging from 20.74 to 22.16 wall units. The stationary case (N=0) varies

from 0.0506 at the pipe wall to 12.4 wall units at the pipe center. However, it varies from 0.0511 at the pipe wall to 12.5 wall units at the pipe center for the highest rotation rate case (N=3). The mesh discerption mentioned above shows that the current grid resolution used in the LES simulations can be considered reasonable.

The computational procedure was performed using a finite difference scheme, which was second-order accurate in space and time. Convective terms were evaluated using Runge-Kutta explicit third-order schemes, while diffusive terms were evaluated using Crank-Nicolson implicit schemes. The time integral was calculated using a fractional step method. The time is made dimensionless using the pipe radius (R) and the maximum velocity of the laminar flow (U_{CL}). A constant *CFL* (Courant, Friedrichs, and Lewy) condition was used in the calculations. The statistics are computed by averaging in the periodic directions and in time. The final data are obtained by ensemble averaging over the time interval from the dimensionless time t =250 until t =8000 for the lowest rotation rate. At the highest rotation rate, the statistics are sampled from the dimensionless time t = 250 until t =10000.

3. Results and discussion:

The current section seeks to analyze and discuss the influence of the rotation cylinder wall on the mean flow and turbulence statistics critically to describe the rheological and hydrodynamic behavior of the swirling flow of pseudoplastic fluid. The emerged LES predictions were validated by comparing some numerical findings results of the shear-thinning and Newtonian fluids with those available in the literature in the following cases: the experimental data of Rudman et al. [16] in the stationery cylinder, the DNS of Rudman et al. [16] for flow behavior index of 0.75 through a stationary cylinder, the experimental data by Reich and Beer [4] for $n=1$ at $N=0,1,3$, the DNS data of Redjem-Saad et al. [29] for $n=1$ at $N=0$, the experimental data by Eggels et al. [7] for Newtonian fluid at $N=0$, and the DNS data of Ould-Rouiss et al. [30] for Newtonian fluid at $N=0,1,3$.

3.1. Apparent viscosity:

The present subsection seeks to reveal the effect of the rotating pipe wall on the different fluid rheological characteristics to describe the rheological behavior of the pseudoplastic fluid. The main emerged rheological properties, such as the apparent fluid viscosity and a shear rate of the shear-thinning, have been critically analysand and discussed in the following paragraphs.

The normalized shear rate $\langle \dot{\gamma} \rangle$ and apparent fluid viscosity $\langle \eta \rangle$ distributions of the shear-thinning (*n=0.75*) and Newtonian (n=1) fluids along the pipe radius (R) are depicted in Fig.2 and Fig.3, respectively, against the distance from the wall-in-wall units Y^+ at a simulation Reynolds number of 4000 and over a rota-

tion rate range of $(0 \le N \le 3)$. It can be seen from Fig.2 that the shear rate of the shear-thinning and Newtonian fluids is nearly linear and remains constant along the viscous sublayer $(0 \le Y^+ \le 5)$ for all rotation rates. The effect of the flow behavior index on the shear rate distributions is significant in the vicinity of the wall, where the shear-thinning profiles lie above those of the Newtonian ones along the near-wall region for all rotation rates. It can be said that the decreased flow behavior index results in a marked increase in the shear rate distributions over the pipe radius. On the other hand, the rotating pipe wall significantly affects the shear rate distributions of both fluids in the viscous sublayer; the increased rotation rate (*N*) induces a pronounced attenuation in the shear rate for the Newtonian fluid.

Beyond approximately Y^+=3, the shear rate profiles begin to drop progressively with the distance from the wall (Y^+) towards the core region, where this reduction is sharped in the buffer region ($5 \le Y^+ \le 30$) for all cases. It is worth noting that the shear rate profiles seem slightly higher with an increasing rotation rate in the logarithmic region; this trend is more pronounced as the rotation rate increases.

It is apparent in Fig.3 that no significant noteworthy difference is observed between the normalized apparent viscosity profile of the shear-thinning ($n=0.75$) fluid for all rotation rates in the near-wall region. In turn, the apparent viscosity profile of the Newtonian fluid is linear and equals the apparent viscosity at the wall along the pipe radius at every rotation rate. It can be said that the apparent viscosity of the pseudoplastic fluid seems independent of the rotation rate (*N*), over the viscous sublayer $(0 \le Y^+ \le 5)$. Beyond the buffer region ($Y^+ > 5$), the apparent viscosity profiles begin to increase gradually far away from the pipe wall towards the core flow region with the distance from the wall (Y^+), there is a clear trend of gradually increasing in the apparent fluid viscosity, where the pseudoplastic (n=0.75) fluid becomes more viscous in the buffer $(5 \le Y^+ \le 30)$ and logarithmic $(30 \le Y^+ \le 200)$ regions. In other words, the pseudoplastic fluid behaves like a solid when approaching the pipe center. On the other hand, it appears that the viscosity profiles of the shear-thinning fluid are slightly affected by the rotating pipe wall; the profiles of the rotating pipe are very close to each other and sensibly higher than the stationary pipe in the buffer layer. As shown in Fig.3, this deviation is more pronounced in the logarithmic region, where the increased rotation rate results in a marked attenuation in the apparent viscosity in this flow region.

Fig.4 presents the distribution of apparent fluid viscosity normalized by viscosity at the wall (η_w) against the shear rate scaled by the shear rate at the pipe wall $(\dot{\gamma}_w)$. The apparent viscosity of the pseudoplastic fluid (n=0.75) is not constant where is a function of the shear rate, where the apparent viscosity of the

pseudoplastic fluid varies with the shear rate along the pipe radius (Fig.4). It is evident that the shear rate attenuates gradually from the wall towards the core region (Fig.2), where this decreased shear rate results in a marked increase in the apparent viscosity of the shear-thinning (Fig.3). Moreover, the apparent viscosity of the pseudoplastic fluid is inversely proportional to the shear rate: the shear rate decreases as the apparent viscosity increases considerably for all rotation rates. Because of the reduced shear rate in the pipe core region, the fluid has a tendency to act more like a solid than a liquid as it moves away from the pipe wall. This causes the viscosity to rise.

On the other hand, with increasing rotation rate, the shear rate and the apparent pseudoplastic viscosity exhibit marked increase and attenuation, respectively, beyond the end of the buffer layer (logarithmic layer), as shown in Fig.2 and Fig.3. It can be said that the increased rotation rate induces in a noticeable increase in the shear rate in the logarithmic region (Fig.2), leading to reduce the apparent viscosity (Fig.3) in the core region. In other words, the pseudoplastic fluid behaves like a liquid approaching the pipe center as the pipe wall rotates (Fig.4).

3.2. Mean velocity profile:

The streamwise velocity profile $U^+ = U/U_\tau$, normalized by the friction velocity $U_\tau = \left(\tau_w/\rho\right)^{1/2}$, is depicted in Fig.5, for $\mathrm{Re}_s = 4000$. At a fixed pipe, the predicted velocity profile is in good agreement with those of Rudman et al. [16] for pseudoplastic fluid and with the experimental results of Eggels et al. [7] and the DNS of Ould-Rouiss et al. [30] and Redjem et al. [29] for a Newtonian fluid. The universal laws in the viscous sublayer and the log region are well predicted for $n = 1$ at $N = 0$. The predicted Newtonian velocity profiles normalized by the mean velocity (U_z / U_b), at various N, Fig.6, agree very well with the experimental results of Reich and Beer [4] and DNS predictions of Ould-Rouiss et al. [30].

When the pipe rotates, the velocity profiles for the shear-thinning fluid, like the Newtonian fluid, deviate from the logarithmic law because of the flow laminarization, Fig.7. Indeed, many investigations results [31], [32], [10], and [30] reported such a deviation from the logarithmic law in the case of a Newtonian fluid. This trend is more pronounced as the rotation rate increases, meaning that the predicted axial velocity profiles have a logarithmic shape $A\ln(Y^+) + B$, where the constants A and B depend on the rotation rate N. This tendency is due to the turbulence level attenuation in the pipe with increasing rotation rate [30]. In the log regions, the predicted velocity for the Newtonian fluid at $N = 3$ is larger than that for the shear-thinning one because the apparent viscosity at $n = 0.75$ is greater than that at $n = 1$. Indeed, the strain $\dot{\gamma}$ decreases towards

the pipe for the shear-thinning fluid, inducing an increase in the apparent viscosity η : the shear-thinning fluid becomes more and more viscous when approaching the pipe center. The fluids become more viscous with decreasing shear rates, which induce a marked higher viscosity, where the pseudoplastic fluid does not flow more quickly towards the pipe center.

The streamwise velocity profile scaled by the centreline velocity versus le radial position, Fig.8, clearly exhibits a turbulence reduction as the rotation rate *N* is increased. At very high *N*, the pseudoplastic mean axial profile gradually approaches the laminar non-Newtonian Poiseuille profile. This is called the laminarization phenomenon. This sort of laminarization has also been observed in the Newtonian fluid and has been pointed out by many researchers [3], [6], [10], and [30]. The LES predictions [33] for *N* up to 18 confirm these trends: the axial velocity profile $n=1$ reaches the laminar parabolic distribution when $N \geq 18$. Note that the axial velocity distribution moves towards the laminar profile more rapidly than $n=1$ when approaching the pipe center because the shear-thinning fluid is more viscous in this region, and thus, the laminarization of the fluid flow is more quickly.

Fig.9 is depicted the tangential mean velocity profiles scaled with the wall rotational velocity. The profiles show a concave shape close to a parabolic curve, and the concavity seems to decrease with increasing rotation rates *N* for both fluids. Similar trends were also observed in the experimental and numerical studies $n=1$ by other authors [5], [4], and [10].

3.3. Turbulence intensity:

Fig.10 and Fig.11 present the evaluations of RMS of velocity fluctuations for the Newtonian and shear-thinning fluids, respectively at $N=0$. The predicted RMS are in satisfactory agreement with the results of Rudman et al. [16] for pseudoplastic fluid and with DNS results [30] and [29] for Newtonian fluid. The slight deviations may be raised because of the difference in the Reynolds value or/and the different numerical methods.

The influence of rotation rate on the RMS of the fluctuating axial velocity U_z' normalized by the friction velocity against the wall distance Y^+ is shown in Fig.12 at various values N . In the non-rotating case, the maximum in the axial velocity fluctuations occurs at a distance $Y^+ \approx 17$ for $n=1$ and $Y^+ \approx 19$ for $n=0.75$. The peak reaches the value of 2.54 for $n=1$ and 2.91 for $n=0.75$. The peak value of 2.54 for the Newtonian fluid and its position $Y^+ \approx 17$ is in accordance with the results of literature [29] and [30]. In the vicinity of the wall, the RMS of the streamwise velocity fluctuations is reduced with increasing rotation rate *N* in the buffer

and log regions (between $Y^+ \approx 5$ and $Y^+ \approx 70$) for $n = 0.75$ and mainly in the buffer region (between $Y^+ \approx 5$ and $Y^+ \approx 35$) for $n = 1$, Fig.12. Beyond the log region, the RMS of the axial velocity is increased with increasing rotation rate. This is because the axial velocity U_z^+ diminishes with increasing rotation rate N for the Newtonian fluid in the buffer region $(5 \le Y^+ \le 35)$ and the shear-thinning fluid in the buffer and log regions $(5 \le Y^+ \le 70)$, see Fig.7, it decreases when *N* raised beyond these regions. Thus, when *N* increases, the turbulent fluctuations are reduced near the wall on a widened zone for $n = 0.75$.

It can be seen that the fluctuations of the axial velocity are larger than the azimuthal and radial ones, Fig.13, Fig.14. It is worth noting that both azimuthal and radial turbulence intensities increase with increasing rotation rate in the vicinity of the wall, the azimuthal up to $Y^+ \approx 10$ for $n = 1$ and $Y^+ \approx 13$ for $n = 0.75$ (which correspond to the peaks of the axial velocity fluctuations). However, beyond these positions, both RMS is increased with increasing N, when N ranges from 0 to 2, and reduced for $N > 2$.

This trend also appears clearly on the turbulent kinetic energy profile, Fig.15. This observation is similar to that reported for the Newtonian case by some authors [30], [10], and [32], who showed, in their numerical investigations, that the turbulence is suppressed for high rotation rates. Note that the wall peaks of the axial velocity RMS, Fig.12, and the turbulent kinetic energy, Fig.15, are reduced until a flat region $N \ge 2$ is achieved. A similar outcome was found by Ould-Rouiss et al. [30] and by Orlandi and Fatica [8] in their numerical simulations for the Newtonian fluid.

The axial-radial distribution of the Reynolds shear stress $\langle U_r' U_z' \rangle$ at $N = 0$ of the shear-thinning fluid agrees reasonably well with the DNS results [16], Fig.16. This stress is the only non-null stress in the stationary pipe. With increasing rotation rate, $\langle U_r' U_z' \rangle$ it is reduced far from the wall, Fig.17, and its distribution is moved to the pipe wall for both fluids, while the stress $\langle U_r' U_\theta' \rangle$ is increased, Fig.18, and the stress $\langle U_z' U_\theta' \rangle$ shows an oscillatory behavior, Fig.19. Near the wall, the peak of $\langle U_z' U_\theta' \rangle$ is related to the tilting of the near-wall vortical structures that increase the amount of correlation between U_z' and U_θ' by [8], Fig.19. Near the rotating wall, higher values of $\langle U_z' U_\theta' \rangle$ the shear-thinning fluid than those for the Newtonian one, especially at $N = 3$ (in comparison to $N = 1$), suggest that the amount of correlation between U_z' and U_θ' is stronger for $n = 0.75$, and it gets stronger and stronger with increase N. Further away from the wall, the normal-wall oscillations of $\langle U_z' U_\theta' \rangle$ becoming noticeable at high rotation rates, and the increased apparent fluid viscosity towards the core region generates larger streamwise vortices at high rotation rates.

3.4. Friction factor:

The friction factor of the pseudoplastic (n=0.75) fluid for the stationary pipe (N=0), is compared to different correlations of the literature for validation (see Tab.2), where f_{DM} f_{FSG} and f_{HR} correspond, respectively, to Dodge and Metzner [13], Gomes [34] and Hanks and Ricks [35] correlations (Tab.2).

$$f_{DM} = a / Re_{MR}^{\ b} \text{ where } a = 0.0665 + 0.01175n \quad b = 0.365 - 0.177n + 0.062n^2$$

$$f_{FSG} = 0.110n^{0.616} Re_{MR}^{-0.287}$$

$$f_{HR} = 0.0682n^{-0.5} / Re_{MR}^{1/(1.87+2.39n)}$$

f_{PG} and f_R, being respectively the LES and DNS predictions by Rudman et al. [16] and Gnambode et al. [17]. The present LES friction factor is in satisfactory agreement with the literature results: it is within 3.8% and 6.5% , respectively, and 15.3% accuracy compared with f_{DM} . The present friction factor is slightly overestimated in comparison to f_{DM} . Rudman et al. [16] reported a similar observation: their predicted friction factor is higher than Dodge and Metzner's correlation [13] by about 10-15% (Tab.2).

For the pseudoplastic fluid (*n=0.75*), table 1 shows a slight diminution of the friction factor when N it varies from 0 to 0.5 and augmentation when. $N \geq 1$, with increasing N . For the pseudoplastic fluid, the augmentation of the rotation rate N induces a rise of the shear stress at the cylinder wall leading to an increase in the friction factor because the fluid becomes more viscous near the wall. As it approaches the cylinder center with increasing rotation pipe wall rate, the attenuation in the apparent fluid viscosity generates less large and less weak axial vortices, leading to less dissipation and increasing the wall drag.

3.5. Visualizations:

The effects of the rotation rate on the resolved axial and radial velocity fluctuations are depicted in Fig.20 and Fig.21, respectively, for pseudoplastic and at the lowest (N=0) and highest (N=3) rotation rates. Contours of the resolved axial velocity in $r-\theta$ a plane at the stationary pipe, Fig.20a, show that the turbulence activity is attenuated in the core region of the pipe where the shear rate is lower (and thus the viscosity higher) than that near the pipe wall. On the contrary, due to the higher shear rate near the wall, the turbulent structures are essentially located close to the pipe wall. In the rotating case, the shear rate is slightly increased (beyond $Y^+ \approx 5$) towards the pipe center (see Fig.2), inducing an augmentation of the turbulent structures in

the core region, Fig.20b, giving a clear picture that the pipe's rotation is responsible for the transport of the fluctuations from the wall towards the core region. A similar picture is given by the contour lines of the radial velocity fluctuations when the rotation rate increases, Fig.21a, Fig.21b. These figures also show that for $N = 3$ (Fig.21b), the number of contour levels U_r' is more than that for $N = 0$ (Fig.21a), which explains the increase of the peak of the RMS of U_r' in Fig.14 when the rotation rate varies from 0 to 3. Indeed, in the core region, the viscosity of the shear-thinning fluid is slightly decreased (see Fig.3) with an increased rotation rate (while the shear rate is slightly increased), inducing a rise of the turbulent structures in the core region and hence an augmentation in radial momentum transfer: the turbulent structures are shorter and stronger and bring more high-speed fluid from the wall region to the core region, reducing the production of turbulent energy near the wall and an increase in the core region (see Fig.15).

4. Conclusions:

In the present work, a large eddy simulation is performed to investigate the turbulent flow of pseudo-plastic fluid in an axially rotating cylinder by using an extended Smagorinsky model. Focus is made on the influence of the rotation rate on the mean flow and turbulence statistics. Results indicated a significant de-pendence of the dynamic field on this parameter. Some of the results are pointed out below:

The centrifugal force induced by the swirl flow induces a marked increase in the shear rate of the pseudoplastic fluid far away from the vicinity of the pipe wall, resulting in a pronounced reduction in the ap-parent viscosity of the shear-thinning fluid in the logarithmic region, where this trend is more noticeable as the rotation rate increases. It should be noted that the variation in the apparent viscosity leads to a redistribution of the axial velocity profile along the pipe radius. The decreased apparent viscosity of the pseudoplastic fluid in the logarithmic layer with an increasing rotating rate results in a gradual increase in the axial velocity profile far away from the pipe wall towards the core region as the pipe wall rotates.

On the other hand, the swirl driven by the rotating pipe wall results in an apparent attenuation in the generation and the transport mechanism of turbulence intensities of the axial velocity fluctuation from the wall vicinity towards the core region for the pseudoplastic fluid. This reduction in the RMS of the axial velocity fluctuations leads to a decrease in the kinetic energy of turbulent fluctuations and, consequently, in the turbu-lent Reynolds shear stress of the axial-radial velocity fluctuations as the pipe wall rotates. In turn, the turbu-lence intensities of the radial and tangential velocity fluctuations exhibit a pronounced increase when the pipe wall is rotating, where this trend is more evident as the rotation rate increases. In other words, the centrifugal force induced by the swirl flow results in a noticeable amelioration in the transport mechanism of the energy

fluctuations from the axial one to the other as the pipe wall rotates. Furthermore, the friction factor for the pseudoplastic fluid exhibits a reduction when the rotation rate varies from 0 to 0.5 and increase when $N \geq 1$ with an increasing rotation rate.

Further studies are needed to study the influence of other rotation rates, flow behavior index ranges, and other effective parameters such as the Reynolds and Prandtl numbers. Moreover, further research could also be conducted to determine the effect of the rotation rate on another model of Non-Newtonian fluids.

Conflict of interest: The author declares that he has no known competing financial interests or personal relationships that could have appeared to influence the work reported in this paper.

References

[1] M. Murakami and K. Kikuyama, "Turbulent Flow in Axially Rotating Pipes," Journal of Fluids Engineering, vol. 102, no. 1, pp. 97–103, Mar. 1980, doi: 10.1115/1.3240633.

[2] K. KIKUYAMA, M. MURAKAMI, K. NISHIBORI, and K. MAEDA, "Flow in an Axially Rotating Pipe : A calculation of flow in the saturated region," Bulletin of JSME, vol. 26, no. 214, pp. 506–513, 1983, doi: 10.1299/jsme1958.26.506.

[3] K. NISHIBORI, K. KIKUYAMA, and M. MURAKAMI, "Laminarization of turbulent flow in the inlet region of an axially rotating pipe.," JSME international journal, vol. 30, no. 260, pp. 255–262, 1987, doi: 10.1299/jsme1987.30.255.

[4] G. Reich and H. Beer, "Fluid flow and heat transfer in an axially rotating pipe—I. Effect of rotation on turbulent pipe flow," International Journal of Heat and Mass Transfer, vol. 32, no. 3, pp. 551–562, Mar. 1989, doi: 10.1016/0017-9310(89)90143-9.

[5] S. Imao, M. Itoh, and T. Harada, "Turbulent characteristics of the flow in an axially rotating pipe," International Journal of Heat and Fluid Flow, vol. 17, no. 5, pp. 444–451, Oct. 1996, doi: 10.1016/0142-727x(96)00057-4.

[6] S. Hirai, T. Takagi, and M. Matsumoto, "Predictions of the Laminarization Phenomena in an Axially Rotating Pipe Flow," Journal of Fluids Engineering, vol. 110, no. 4, pp. 424–430, Dec. 1988, doi: 10.1115/1.3243573.

[7] S. W. Tu and B. R. Ramaprian, "Fully developed periodic turbulent pipe flow. Part 1. Main experimental results and comparison with predictions," Journal of Fluid Mechanics, vol. 137, pp. 31–

58, Dec. 1983, doi: 10.1017/s0022112083002281.

[8] P. ORLANDI and M. FATICA, “Direct simulations of turbulent flow in a pipe rotating about its axis,” Journal of Fluid Mechanics, vol. 343, pp. 43–72, Jul. 1997, doi: 10.1017/s0022112097005715.

[9] Z. Yang, “Large eddy simulation of fully developed turbulent flow in a rotating pipe,” International Journal for Numerical Methods in Fluids, vol. 33, no. 5, pp. 681–694, 2000, doi: 3.0.co;2-a">10.1002/1097-0363(20000715)33:5<681::aid-fld25>3.0.co;2-a.

[10] A. A. Feiz, M. Ould-Rouis, and G. Lauriat, “Turbulence Statistics in a Fully Developed Rotating Pipe Flow,” Journal of Enhanced Heat Transfer, vol. 12, no. 3, pp. 273–288, 2005, doi: 10.1615/jenhheattransf.v12.i3.50.

[11] A. B. Metzner and J. C. Reed, “Flow of non-newtonian fluids—correlation of the laminar, transition, and turbulent-flow regions,” AIChE Journal, vol. 1, no. 4, pp. 434–440, Dec. 1955, doi: 10.1002/aic.690010409.

[12] A. B. Metzner, “Non-Newtonian Fluid Flow. Relationships between Recent Pressure-Drop Correlations,” Industrial & Engineering Chemistry, vol. 49, no. 9, pp. 1429–1432, Sep. 1957, doi: 10.1021/ie50573a049.

[13] D. W. Dodge and A. B. Metzner, “Turbulent flow of non-newtonian systems,” AIChE Journal, vol. 5, no. 2, pp. 189–204, Jun. 1959, doi: 10.1002/aic.690050214.

[14] F. T. Pinho and J. H. Whitelaw, “Flow of non-Newtonian fluids over a confined baffle,” Journal of Fluid Mechanics, vol. 226, pp. 475–496, May 1991, doi: 10.1017/s0022112091002471.

[15] M. R. Malin, “Turbulent pipe flow of power-law fluids,” *Int. Commun. Heat Mass Transf.*, vol. 24, no. 7, pp. 977–988, Nov. 1997.

[16] M. Rudman, H. M. Blackburn, L. J. W. Graham, and L. Pullum, “Turbulent pipe flow of shear-thinning fluids,” Journal of Non-Newtonian Fluid Mechanics, vol. 118, no. 1, pp. 33–48, Mar. 2004, doi: 10.1016/j.jnnfm.2004.02.006.

[17] P. S. Gnambode, P. Orlandi, M. Ould-Rouiss, and X. Nicolas, “Large-Eddy simulation of turbulent pipe flow of power-law fluids,” International Journal of Heat and Fluid Flow, vol. 54, pp. 196–210, Aug. 2015, doi: 10.1016/j.ijheatfluidflow.2015.05.004.

[18] A. A. Gavrilov and V. Ya. Rudyak, “Direct numerical simulation of the turbulent flows of power-law fluids in a circular pipe,” Thermophysics and Aeromechanics, vol. 23, no. 4, pp. 473–486, Jul. 2016, doi: 10.1134/s0869864316040016.

[19] A. A. Gavrilov and V. Ya. Rudyak, “Direct numerical simulation of the turbulent energy balance and the shear stresses in power-law fluid flows in pipes,” Fluid Dynamics, vol. 52, no. 3, pp. 363–374, May 2017, doi: 10.1134/s0015462817030048.

[20] J. Singh, M. Rudman, and H. M. Blackburn, “Reynolds number effects in pipe flow turbulence of generalized Newtonian fluids,” Physical Review Fluids, vol. 3, no. 9, Sep. 2018, doi: 10.1103/physrevfluids.3.094607.

[21] J. Singh, M. Rudman, and H. M. Blackburn, “The effect of yield stress on pipe flow turbulence for generalised newtonian fluids,” Journal of Non-Newtonian Fluid Mechanics, vol. 249, pp. 53–62, Nov. 2017, doi: 10.1016/j.jnnfm.2017.09.007.

[22] E. Z. Zheng, M. Rudman, J. Singh, and S. B. Kuang, “Direct numerical simulation of turbulent non-Newtonian flow using OpenFOAM,” Applied Mathematical Modelling, vol. 72, pp. 50–67, Aug. 2019, doi: 10.1016/j.apm.2019.03.003.

[23] V. Vidyanidhi and A. Sithapathi, “Non-Newtonian Flow in a Rotating Straight Pipe,” Journal of the Physical Society of Japan, vol. 29, no. 1, pp. 215–219, Jul. 1970, doi: 10.1143/jpsj.29.215.

[24] R. W. Gunn, B. Mena, and K. Walters, “On Newtonian and non-Newtonian flow in a rotating pipe,” Zeitschrift für angewandte Mathematik und Physik ZAMP, vol. 25, no. 5, pp. 591–606, Sep. 1974, doi: 10.1007/bf01596121.

[25] M. Abdi, A. Noureddine, and M. Ould-Rouiss, “Numerical simulation of turbulent forced convection of a power law fluid flow in an axially rotating pipe,” Journal of the Brazilian Society of Mechanical Sciences and Engineering, vol. 42, no. 1, Dec. 2019, doi: 10.1007/s40430-019-2099-7.

[26] T. Ohta and M. Miyashita, “DNS and LES with an extended Smagorinsky model for wall turbulence in non-Newtonian viscous fluids,” Journal of Non-Newtonian Fluid Mechanics, vol. 206, pp. 29–39, Apr. 2014, doi: 10.1016/j.jnnfm.2014.02.003.

[27] E. Montreuil, “Simulation numérique pour l’aérothermique avec des modèles sous-maille,” Oct. 2000.

[28] T. A. Zang, “Numerical Simulation of the Dynamics of Turbulent Boundary Layers: Perspectives of a Transition Simulator,” *Philos. Trans. R. Soc. A Math. Phys. Eng. Sci.*, vol. 336, no. 1641, pp. 95–102, Aug. 1991.

[29] L. Redjem-Saad, M. Ould-Rouiss, and G. Lauriat, “Direct numerical simulation of turbulent heat transfer in pipe flows: Effect of Prandtl number,” International Journal of Heat and Fluid Flow, vol. 28, no. 5, pp. 847–861, Oct. 2007, doi: 10.1016/j.ijheatfluidflow.2007.02.003.

[30] M. Ould-Rouiss, A. Dries, and A. Mazouz, “Numerical predictions of turbulent heat transfer for air flow in rotating pipe,” International Journal of Heat and Fluid Flow, vol. 31, no. 4, pp. 507–517, Aug. 2010, doi: 10.1016/j.ijheatfluidflow.2010.02.015.

[31] Y. Zhang, A. Gandhi, A. G. Tomboulides, and S. A. Orszag, “Simulation of pipe flow,” *Appl. direct large eddy Simul. to Transit. Turbul.*, pp. 11–17, 1994.

[32] P. Orlandi and D. Ebstein, “Turbulent budgets in rotating pipes by DNS,” International Journal of Heat and Fluid Flow, vol. 21, no. 5, pp. 499–505, Oct. 2000, doi: 10.1016/s0142-727x(00)00037-0.

[33] M. Ould-Rouiss and A. Feiz, “Numerical simulation of turbulent pipe flow,” in *Fluid Mechanics and Pipe Flow: Turbulence, Simulation and Dynamics*, D. Matos and C. Valerio, Eds. Nova Publishers, 2009, p. 231 268.

[34] F. Gomes, “Hydraulic, Power Law models, calculation method using rational polynomial models,” *Tech. Meet. Softw. Dev. Drill. Oper. CAPER/87, Salvador. Brazil,(in Port.*, 1987.

[35] R. W. Hanks and B. L. Ricks, “Transitional and Turbulent Pipeflow of Pseudoplastic Fluids,” *J. Hydronautics*, vol. 9, no. 1, pp. 39–44, Jan. 1975.

NOMENCLATURE

U_b	Average velocity, $\left(m.s^{-1}\right)$
U_τ	Friction velocity $U_\tau = \left(\tau_w/\rho\right)^{1/2}$, $\left(m.s^{-1}\right)$
U_{CL}	Centreline axial velocity for analytical fully developed laminar profile $U_{CL} = \left(3n+1\right)U_b/\left(n+1\right)$, $\left(m.s^{-1}\right)$
R	Pipe radius, $\left(m\right)$
n	Flow index
K	Consistency index $\left(pa.s^n\right)$
k	Turbulent kinetic energy
Y^+	Distance from the wall in wall unites $Y^+ = \rho U_\tau \left(r-R\right)/\eta_w$
Ω_k	Rotational velocity of the pipe wall
N_k	Rotation rate $N_k = 2\Omega_k R/U_{CL}$
f	Mean friction factor $f = 2\tau_W/\left(\rho U_b{}^2\right)$

$\bar{S}_{ij}$	Strain rate tensor $\bar{S}_{ij} = 1/2\left(\partial\bar{u}_i/\partial x_j + \partial\bar{u}_j/\partial x_i\right)$
Re_s	Reynolds number of the simulations $\mathrm{Re}_s = \rho U_{CL}{}^{2-n} R^n / K$
Re_{MR}	Metzner-Reed Reynolds number $\mathrm{Re}_{MR} = 8\rho U_b{}^{2-n} / K\left(6+2/n\right)^n$
Re_g	Generalized Reynolds number $\mathrm{Re}_g = \rho U_b D/\eta_W$
Re_{cr}	Critical Reynolds number $\mathrm{Re}_{cr} = 2100\left(\left(4n+2\right)\left(5n+3\right)/3\left(3n+1\right)^2\right)$

Greek symbols	
$\dot{\gamma}$	Shear rate $\dot{\gamma} = \sqrt{S_{ij}S_{ij}}\ \left(s^{-1}\right)$
Δ	Computational grid
η	apparent viscosity $\eta = K\dot{\gamma}^{n-1}\ \left(Kg.s^{-1}\right)$
ρ	Density $\left(Kg.m^{-3}\right)$
$\bar{\tau}_{ij}$	Subgrid stress tensor $\bar{\tau}_{ij} = -2\nu_t\bar{S}_{ij}$

Subscripts	
d	Dimensionless
z, r, θ	Axial, radial, tangential velocity
b	Average
C	Centreline
L	Laminar
t	Turbulent
s	Simulation
w	Wall
g	Generalized

Superscripts	
$\langle\ \rangle$	Statistically averaged
$(\ )^+$	Normalized by U_τ, or T_τ
$(\ )'$	Fluctuation component
$\left(\bar{\ }\right)$	Filtered variable

Table 1: parameters of present LES simulations and mean flow quantities for $n = 0.75$ and $\mathrm{Re}_s = 4000$

N	0	0.5	1	2	3
Δz^+	69.89	66.01	67.76	68.61	70.55
$r\Delta\theta^+$	21.95	20.74	21.29	21.55	22.16
$\Delta r^+_{\min}$	0.0506	0.0478	0.0491	0.0497	0.0511
$\Delta r^+_{\max}$	12.4	11.71	12	12.17	12.5
U_b/U_{cl}	0.5329	0.5312	0.5304	0.5287	0.5278
U_c/U_{cl}	0.6863	0.7542	0.7947	0.8688	0.9048
$U_\tau/U_{cl}.10^1$	0.3393	0.3278	0.333	0.3355	0.3412
$\dot{\gamma}_{d,w}$	6.6818	8.0258	6.770	6.6340	8.210
$\eta_{d,w}$	0.6334	0.6069	0.6315	0.6305	0.6036
Re_{cr}	2250	2250	2250	2250	2250
Re_s	4000	4000	4000	4000	4000
Re_{MR}	4873.2	4854.2	4845.6	4826.1	4815.4
Re_g	7135.8	6953	7016	7028.2	7094.3
Re_τ	227.16	214.56	220.24	222.99	229.29
Y_1^+	0.0239	0.0226	0.0232	0.0235	0.0241
$f.10^3$	9.2099	8.6003	8.8741	9.0072	9.3133

Table 2: Friction factor at $\mathrm{Re}_s = 4000$

$f.10^3$	$f_{DM}.10^3$	$f_{FSG}.10^3$	$f_{HR}.10^3$	$f_{PG}.10^3$	$f_R.10^3$
9.20	7. 79	8.05	7.75	8.85	8.6

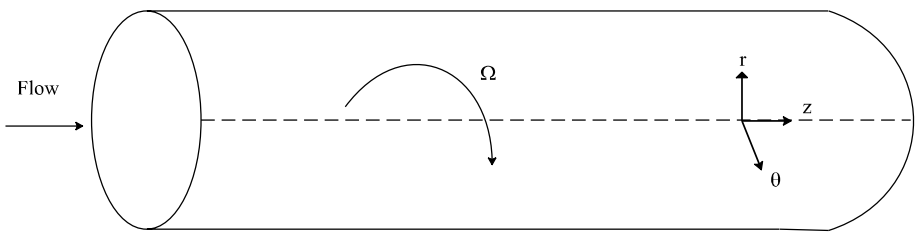

Fig. 1: Geometry of problem

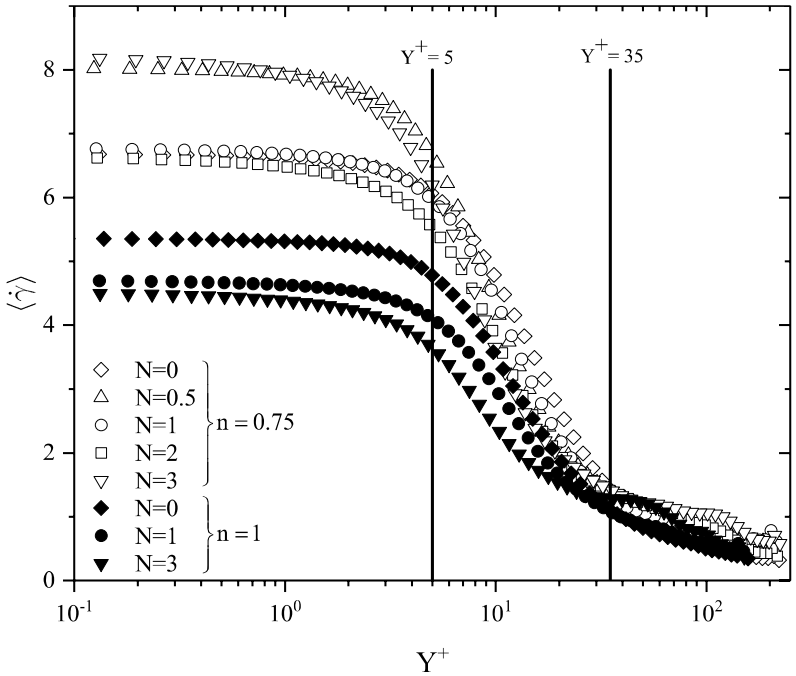

Fig. 2: Behaviour of mean dimensionless shear rate

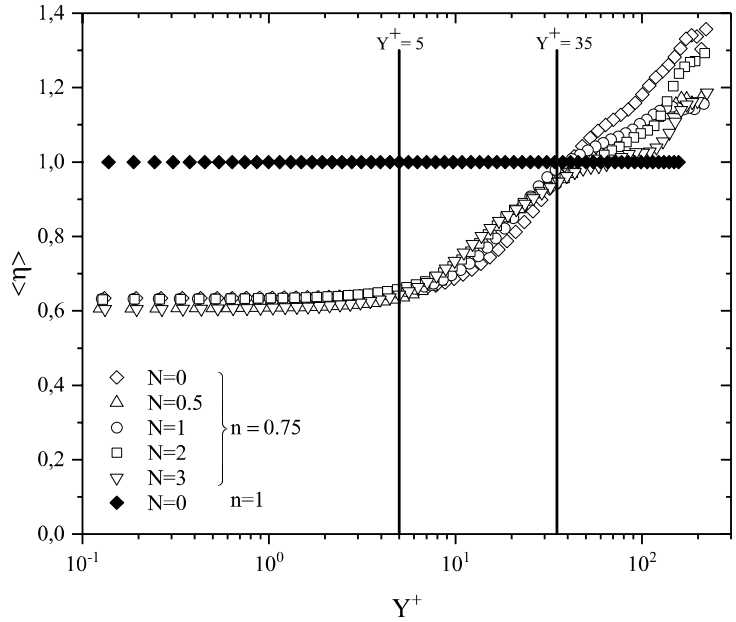

Fig. 3: Apparent viscosity behaviour

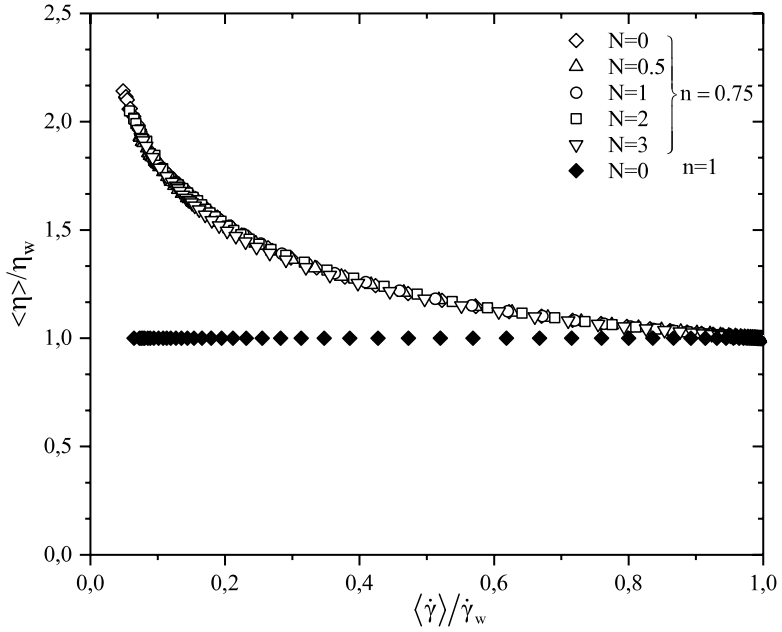

Fig. 4: Normalised apparent viscosity behavior

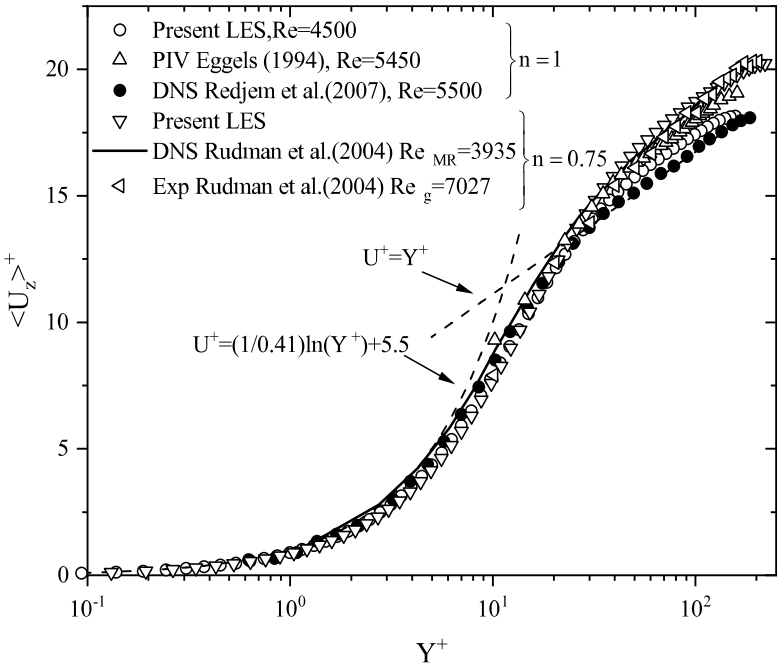

Fig. **5:** Turbulent axial velocity

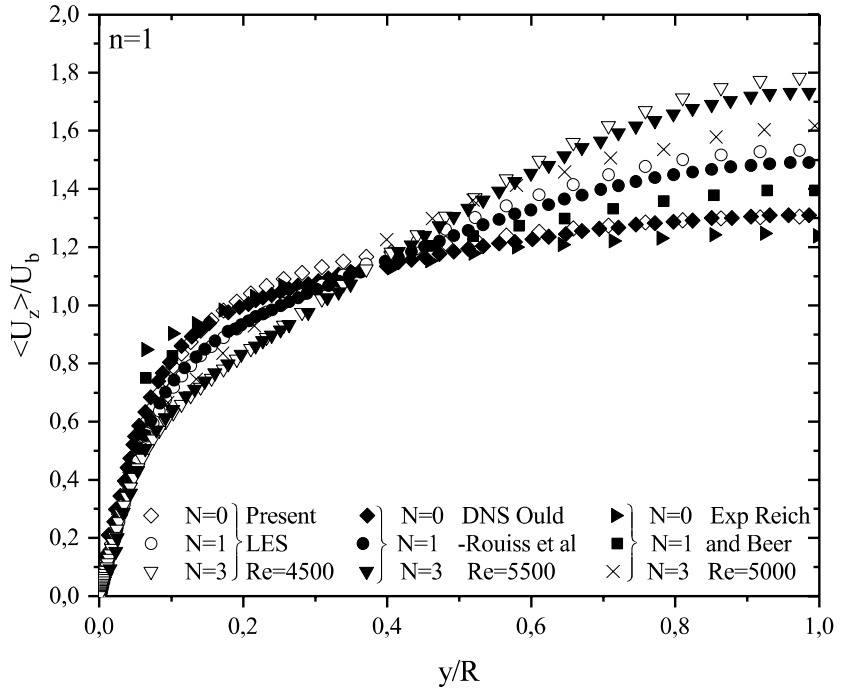

Fig. 6: Axial velocity distribution

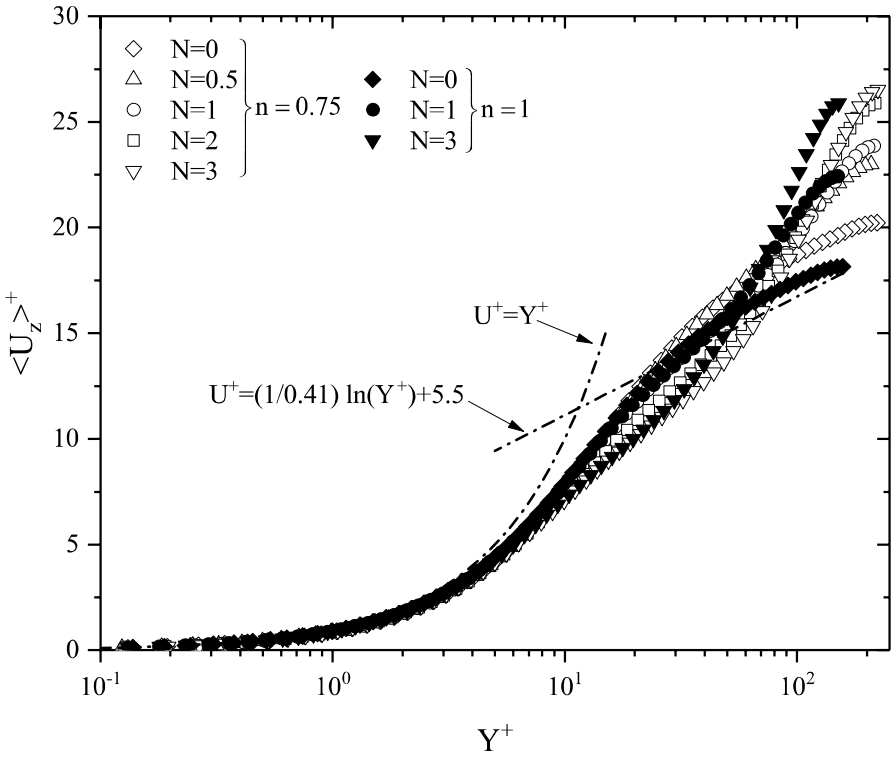

Fig. 7: Turbulent axial velocity profile

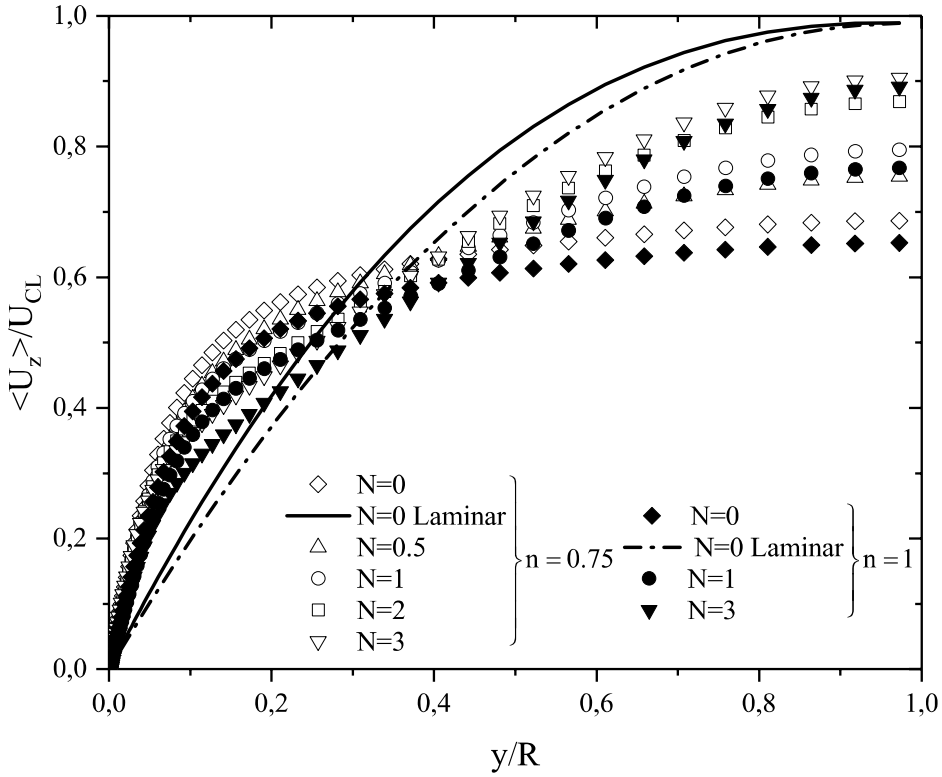

Fig. 8: Mean streamwise velocity distribution

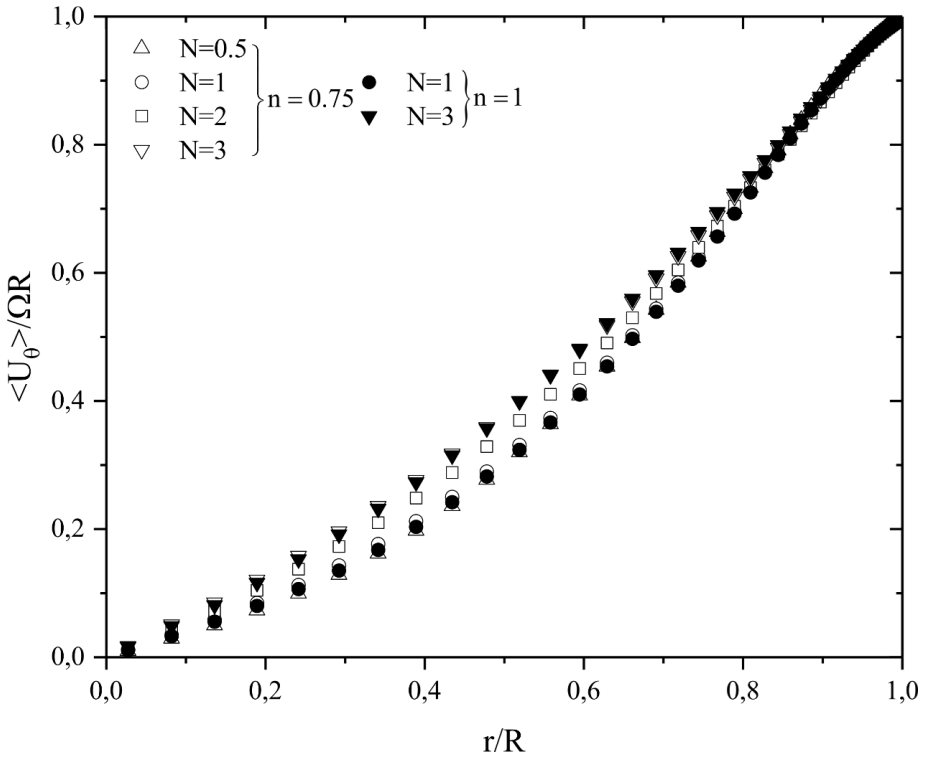

Fig. 9: Tangential velocity distribution

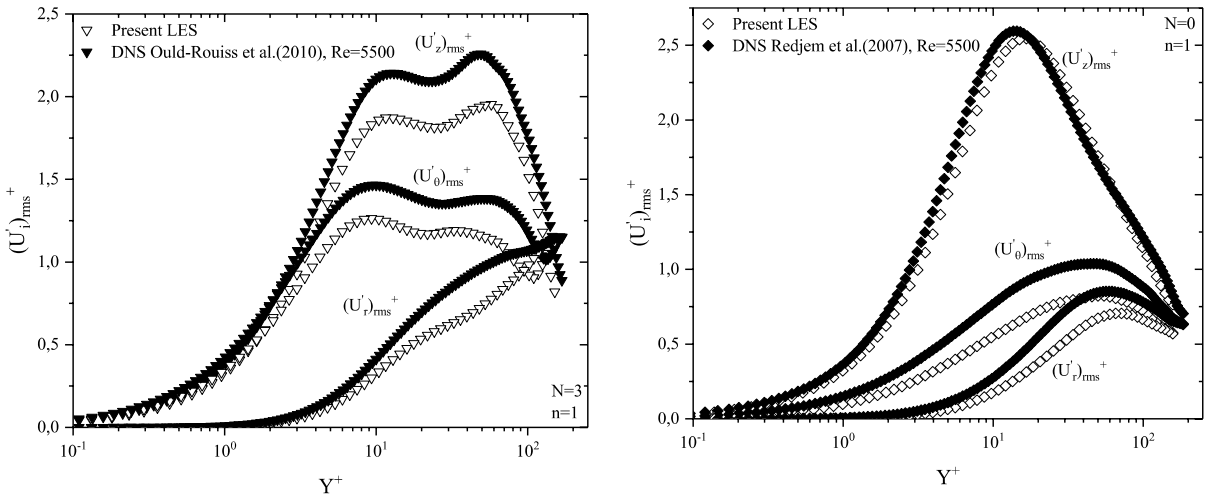

(a) (b)

Fig. 10: Validation of Turbulence intensity (Newtonian)

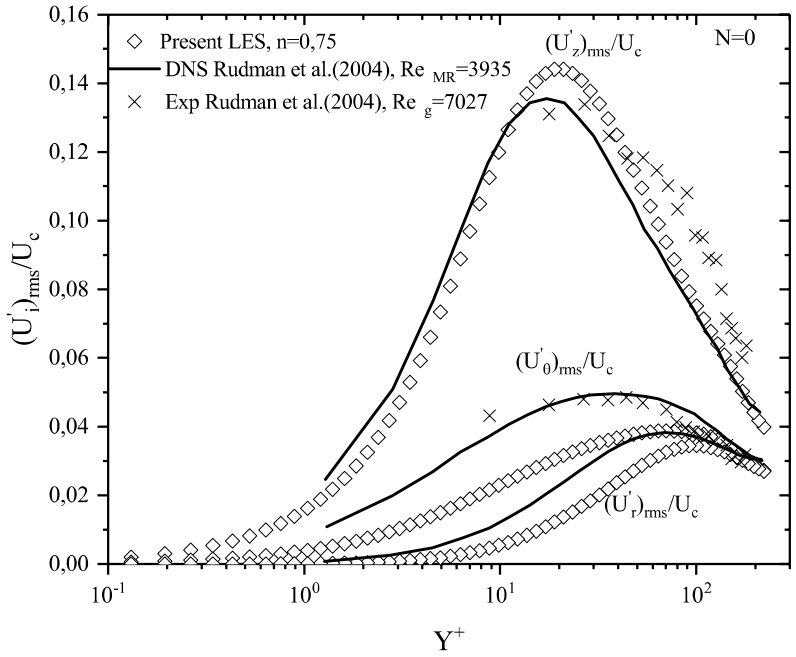

Fig. 11: Validation of Turbulence intensity (Pseudoplastic)

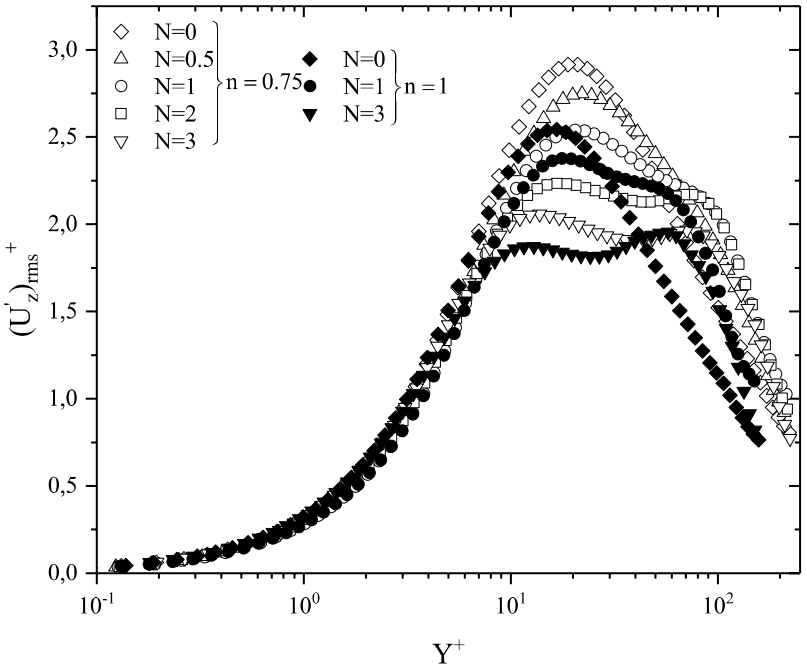

Fig. 12: RMS of axial velocity fluctuations

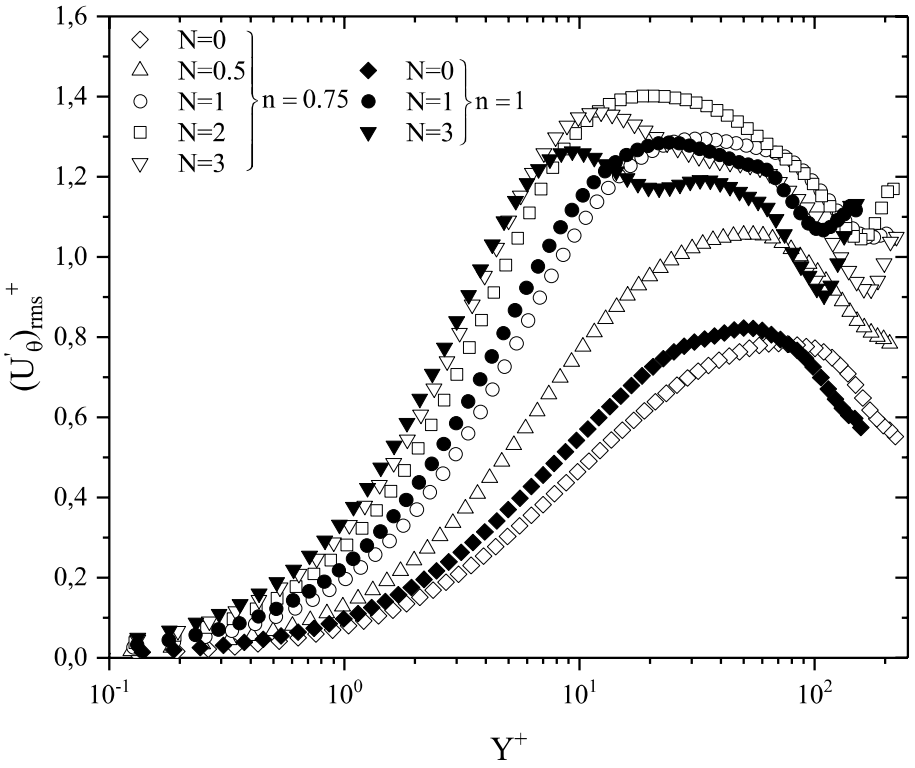

Fig. 13: RMS of tangential velocity fluctuations profile

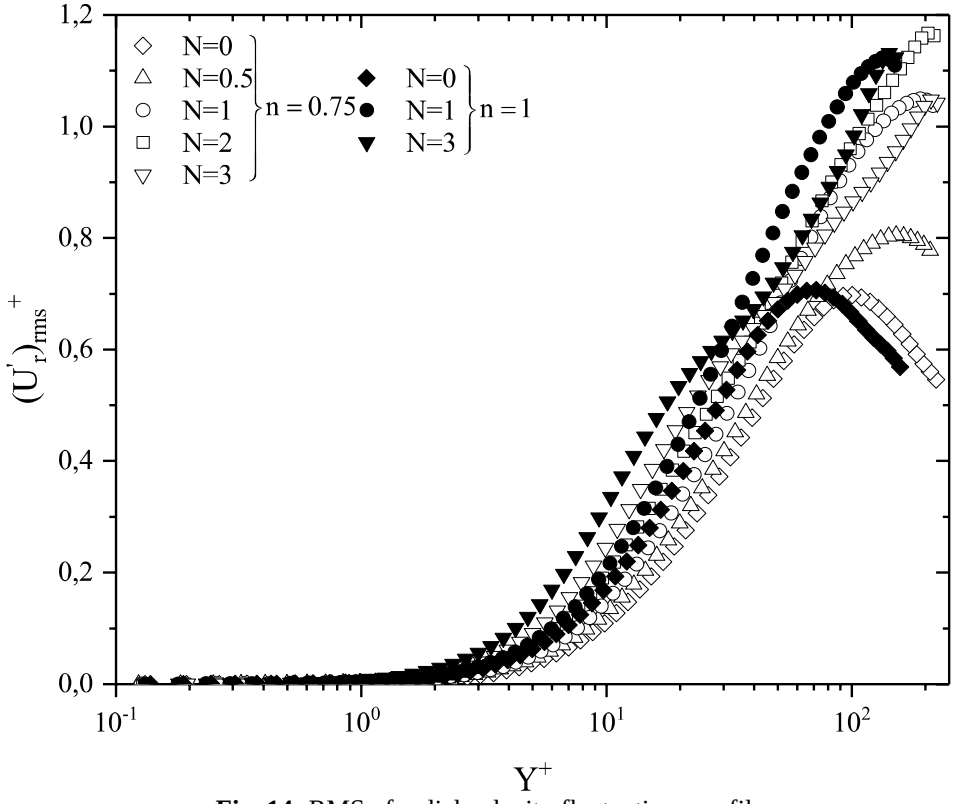

Fig. 14: RMS of radial velocity fluctuations profile

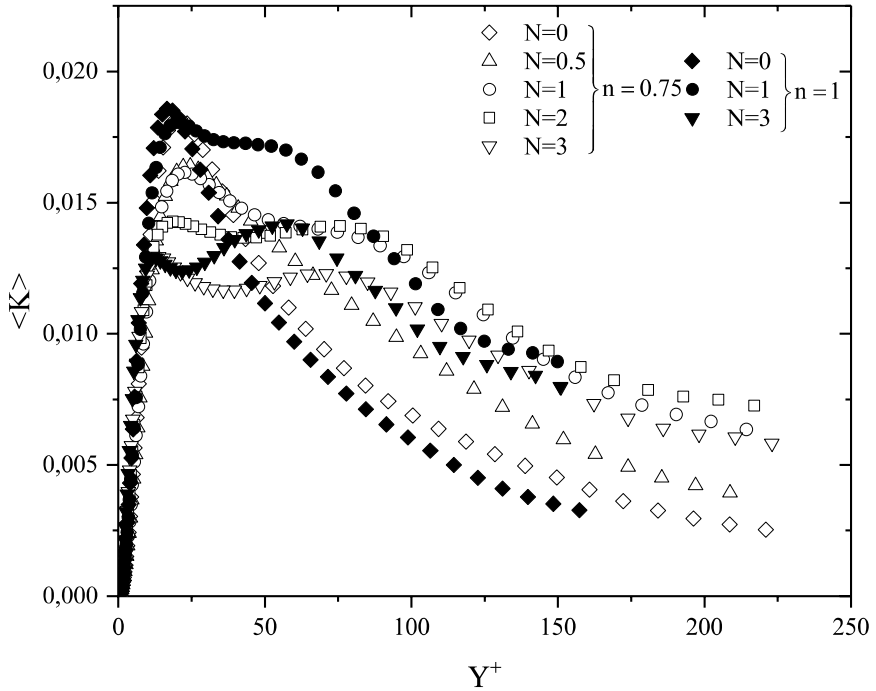

Fig. 15: Distribution of the turbulent kinetic energy

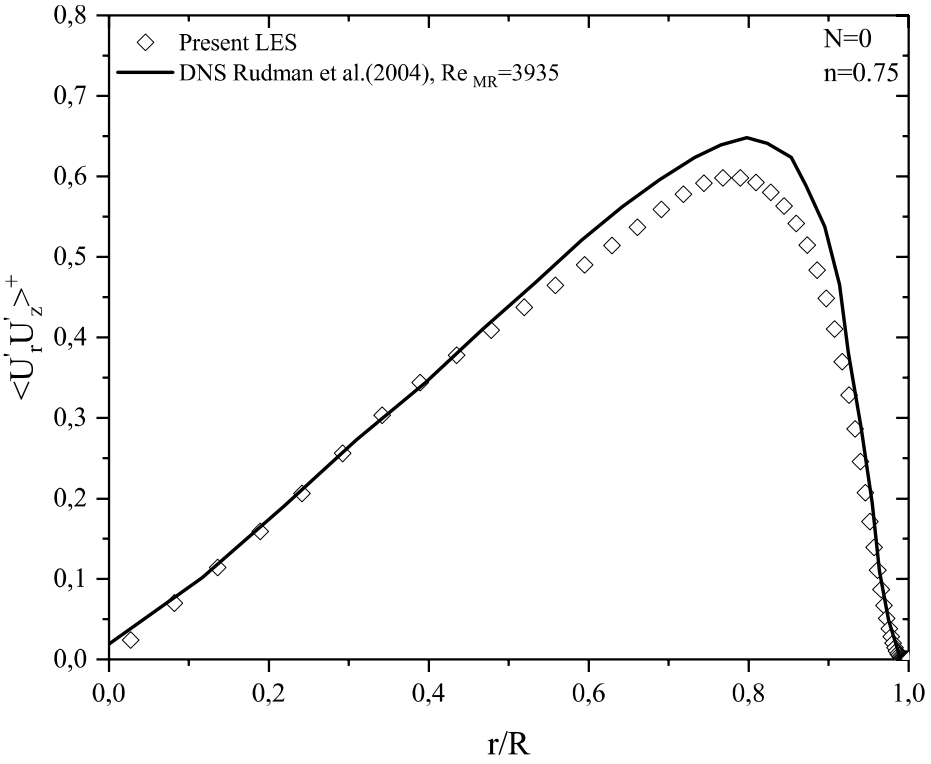

Fig. 16: Validation of Reynolds shear stress

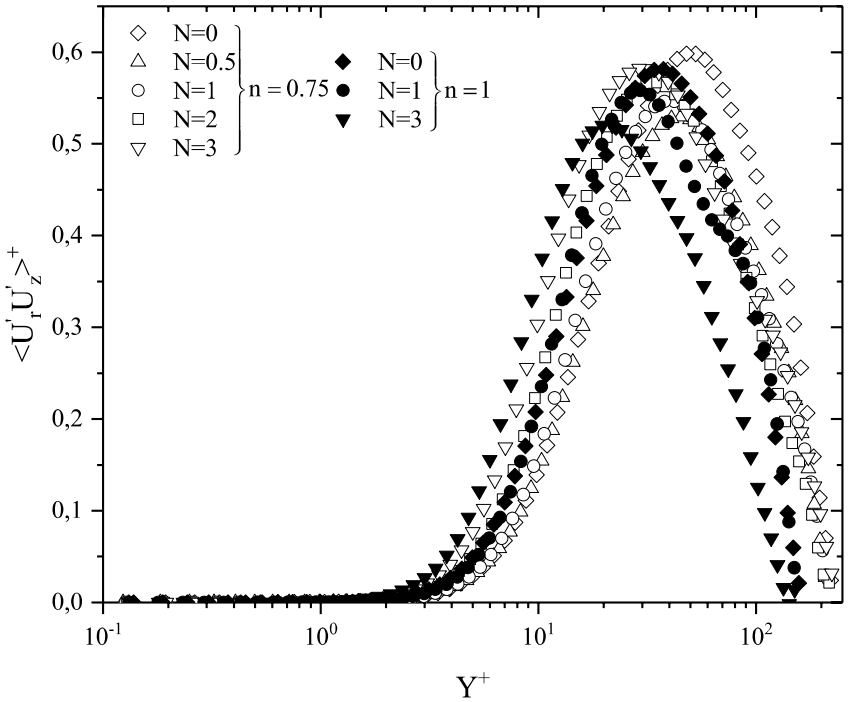

Fig. 17: Reynolds shear stress of normal-wall and streamwise velocity fluctuations

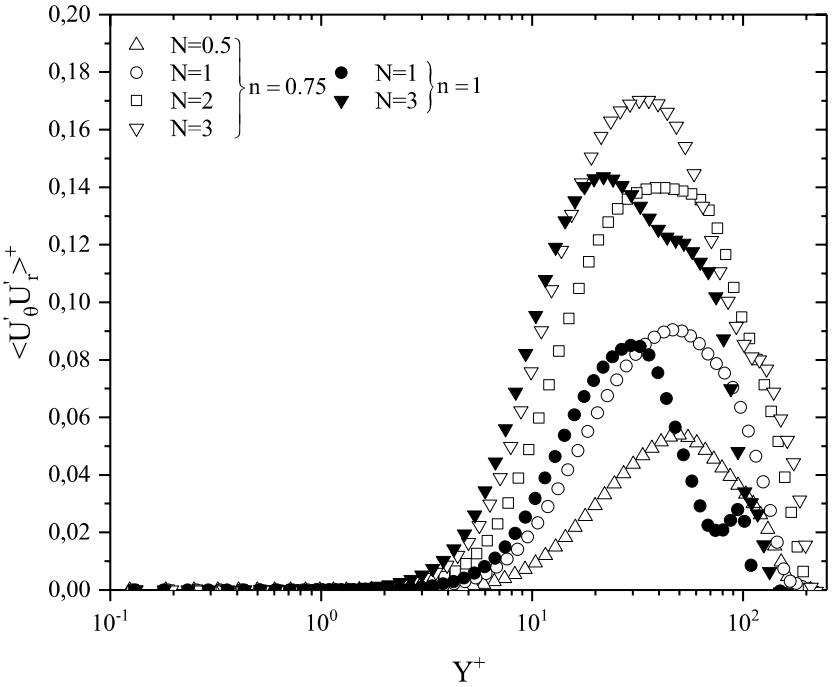

Fig. 18: Reynolds shear stress of tangential and normal-wall velocity fluctuations

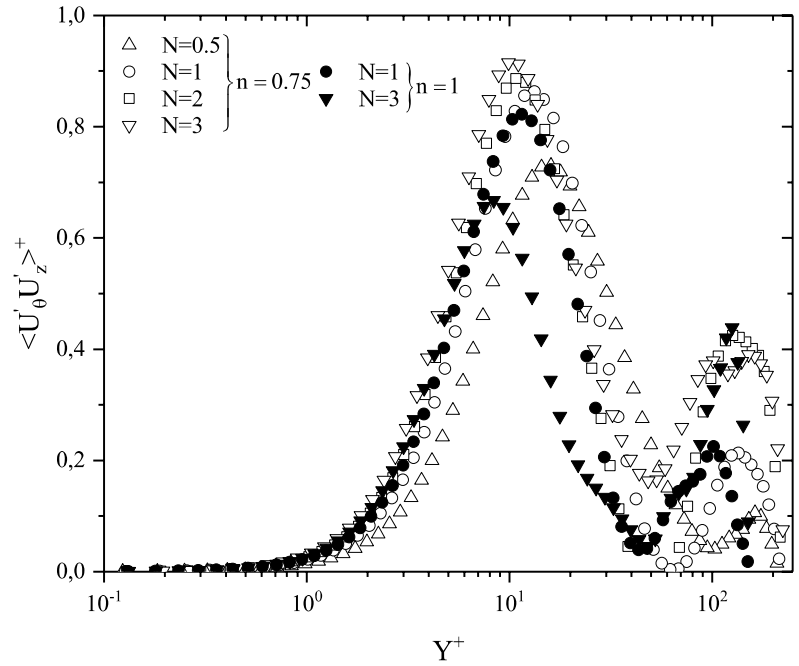

Fig. 19: Reynolds shear stress of tangential and axial velocity fluctuations

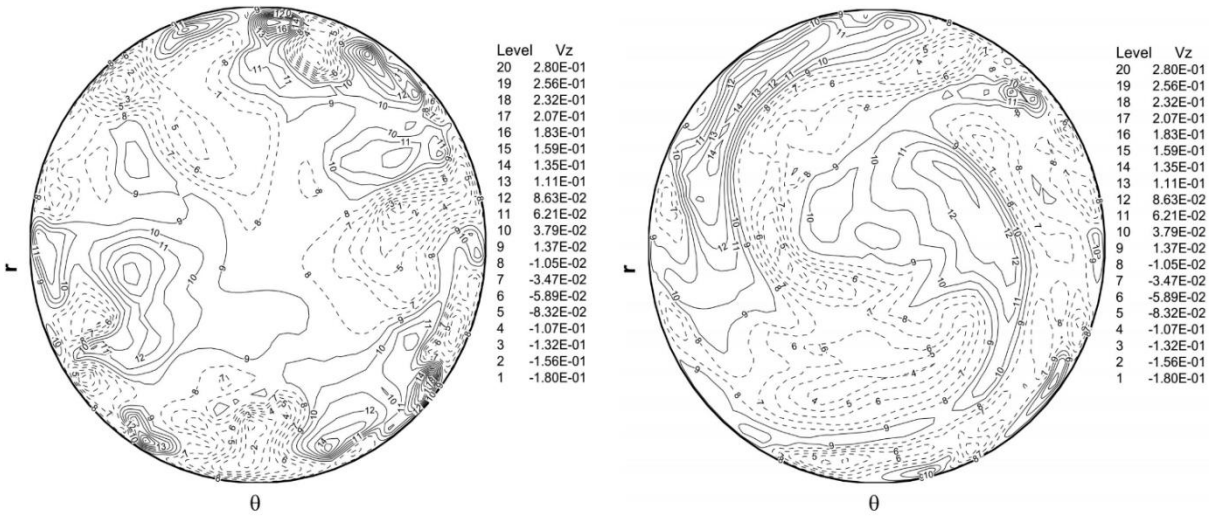

(a) N=0 (b) N=3

Fig. 20: Contour lines of the axial velocity fluctuations

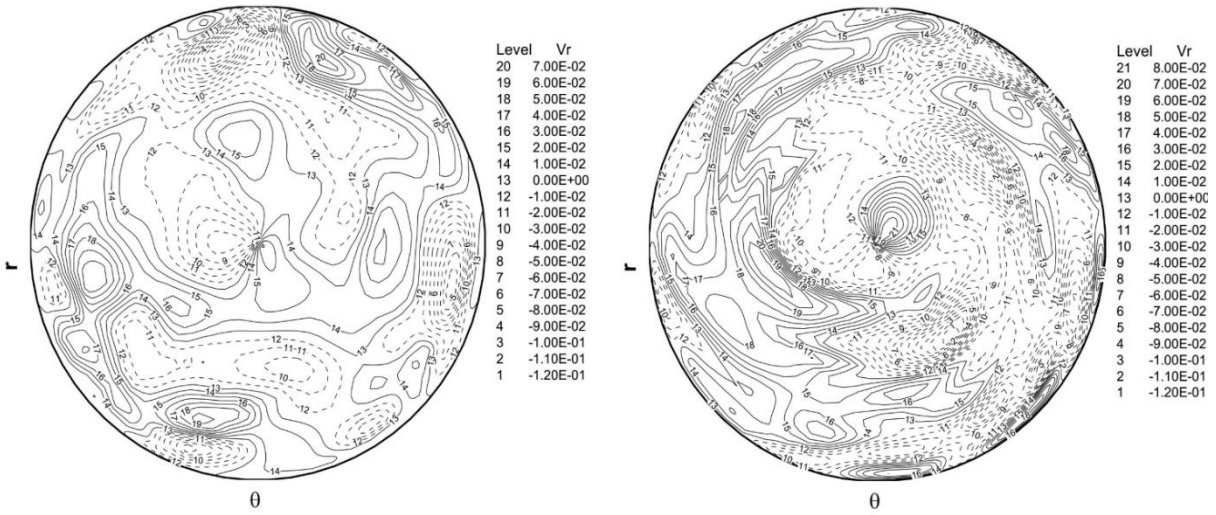

(a) N=0 (b) N=3

Fig. 21: Contour lines of the radial velocity fluctuations

List of figures